
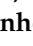


Article

Metallacrown of $\text{Ce}^{\text{III}}\text{Cu}^{\text{II}}_5$: Synthesis, Structural Characterization and Insights for Nanoparticles [†]

Jésio D. Tempesta ¹, Fábio Faria Paiva ¹, Leonildo A. Ferreira ², Rafaela M. R. da Silva ¹ ,
Luckerman D. G. Botelho ¹ , Iara M. L. Rosa ¹, Caio Cesar Candido ³ , Angelo Marcio Gomes ⁴ ,
Wallace C. Nunes ⁵ , Guilherme P. Guedes ⁶  and Maria Vanda Marinho ^{1,*} 

- ¹ LaPI, Instituto de Química, Universidade Federal de Alfenas, Campus Santa Clara, Alfenas 37133-840, MG, Brazil; jesio.tempesta@sou.unifal-mg.edu.br (J.D.T.); fabio.faria.paiva@gmail.com (F.F.P.); rafaela.silva@sou.unifal-mg.edu.br (R.M.R.d.S.); luckerman.botelho@sou.unifal-mg.edu.br (L.D.G.B.); cristalografia.landre@gmail.com (I.M.L.R.)
² Instituto de Química, Universidade Federal de Goiás, Campus Samambaia, Goiânia 74690-900, GO, Brazil; leonildoferreira@ufg.br
³ LabcrystAL, Instituto de Química, Universidade Federal de Alfenas, Campus Santa Clara, Alfenas 37133-840, MG, Brazil; caio.candido@sou.unifal-mg.edu.br
⁴ Instituto de Física, Universidade Federal do Rio de Janeiro, Cidade Universitária, Rio de Janeiro 21941-972, RJ, Brazil; amgomes@if.ufrj.br
⁵ Instituto de Física, Universidade Federal Fluminense, Niterói 24210-346, RJ, Brazil; wcnunes@id.uff.br
⁶ Instituto de Química, Universidade Federal Fluminense, Niterói 24020-141, RJ, Brazil; guilherme_guedes@id.uff.br
* Correspondence: maria.marinho@unifal-mg.edu.br
[†] M. V. Marinho dedicates this article to the beloved memory of the great friend and Professor Miguel Julve.
[‡] Dedicated to the brilliant careers of M. Julve and F. Lloret.



Citation: Tempesta, J.D.; Paiva, F.F.; Ferreira, L.A.; da Silva, R.M.R.; Botelho, L.D.G.; Rosa, I.M.L.; Candido, C.C.; Gomes, A.M.; Nunes, W.C.; Guedes, G.P.; et al. Metallacrown of $\text{Ce}^{\text{III}}\text{Cu}^{\text{II}}_5$: Synthesis, Structural Characterization and Insights for Nanoparticles. *Magnetochemistry* **2024**, *10*, 96. <https://doi.org/10.3390/magnetochemistry10120096>

Academic Editors: Carlos J. Gómez García and Salah-Eddine Stiriba

Received: 1 November 2024

Revised: 26 November 2024

Accepted: 27 November 2024

Published: 30 November 2024



Copyright: © 2024 by the authors. Licensee MDPI, Basel, Switzerland. This article is an open access article distributed under the terms and conditions of the Creative Commons Attribution (CC BY) license (<https://creativecommons.org/licenses/by/4.0/>).

Abstract: The heterobimetallic 15-MC-5 metallacrown of formula $[\text{CeCu}_5(5\text{mpzHA})_5(\text{NO}_3)(\text{H}_2\text{O})_7]\cdot 2\text{NO}_3\cdot 7\text{H}_2\text{O}$, designated **MC-Ce**, was synthesized using 5-methyl-2-pyrazinehydroxamic acid (5mpzHA) as a linker, reacting with Ce^{III} and Cu^{II} salts under mild conditions. Single-crystal X-ray diffraction analysis reveals a crown-like $[\text{Cu}_5\text{Ce}(5\text{mpzHA})_5]$ core, characteristic of a 15-MC-5 system, with five Cu^{II} atoms at the rim of the crown and the Ce^{III} ion occupying the dome of the crown, with water molecules, oxygen atoms and one nitrate anion filling the nine-coordination sphere around the Ce^{III} ion, which exhibits a distorted spherical tricapped trigonal prism geometry. The thermogravimetric analysis evidences successive mass losses due to the removal of water molecules and decomposition of the structure after 217 °C, whereas the PXRD analysis of the thermal decomposition residue reveals the presence of copper and copper/cerium oxide particles. These nanocomposite materials were also synthesized using the metallacrown **MC-Ce** under a hydrothermal method in the presence of multi-walled carbon nanotubes (MWCNTs), affording insights that this metallacrown can act as a source precursor for the synthesis of these mixed cerium/copper oxide nanomaterials. The experimental χ_{MT} value in **MC-Ce** at room temperature is 3.175 cm³ mol^{−1} K, which is higher than the calculated one for one magnetically isolated Ce^{III} plus five Cu^{II} ions, probably due to the antiferromagnetic interactions among Cu^{II} ions within the metallacrown hoop plus the thermal depopulation of J_Z sublevels of Ce^{III} ground state (5/2), which exhibit a small splitting under the anisotropic ligand field effects. The χ_{MT} decreases continuously until it reaches the value of 0.80 cm³ mol^{−1} K at 10 K, reinforcing the presence of intramolecular antiferromagnetic interactions.

Keywords: 3d–4f metallacrown; cerium and copper oxide nanoparticles; magnetic properties

1. Introduction

Metallacrowns (MCs) are structures containing a cyclic core formed by repeating $-\text{[M-N-O]}_n-$ units with an X-MC-Y topological representation [1] that have been developed very rapidly within the metallamacrocyclic field [2]. The scope of the size of MCs in the

solid state built by the Cu^{II} center, for example, has been found to be 9-MC-3, 12-MC-4, Ln^{III} [15-MC-5], and Ln^{III} [18-MC-6], as summarized by M. V. Marinho et al. [3]. We have focused on MC chemistry with one particular 15-metallacrown-5 [3], assembled by the reaction between 5-methyl-2-pyrazinehydroxamic acid (5mpzHA) with copper(II) and europium(III) salts.

Examining the formation of MCs based on the Ce^{III} ion into the MC ring, there are only two examples [4,5], and even though it is well known that the Ce^{III} ion has only one unpaired electron, $4f^1$, the expected ground state ($L = 3$, and $S = 1/2$) is $^2F_{5/2}$, [6] which contributes to its striking feature of magnetic anisotropy [7]. Interestingly Ce^{III} -based SMMs are found [7–10], as well as templates for the synthesis of copper and cerium oxide nanoparticles [4,5], which opened new avenues for applications in sensors, fuel cells, coatings, and catalysts. [5]

Thus, in this contribution, we present the synthesis, results of thermal analysis, and spectroscopic, X-ray diffraction, and magnetic properties of a 15-MC-5 metallacrown of formula $[\text{CeCu}_5(5\text{mpzHA})_5(\text{NO}_3)(\text{H}_2\text{O})_7] \cdot 2\text{NO}_3 \cdot 7\text{H}_2\text{O}$ (**MC-Ce**). In addition, we prepared nanocomposites of cerium and copper oxides supported on multi-walled carbon nanotubes (MWCNTs) under hydrothermal conditions, using water as the sole solvent in a stainless-steel autoclave at 190 °C. This synthetic approach was motivated by the nature of the metallacrown precursor **MC-Ce**, which contains metal–oxygen bonds with required metal atoms and undergoes thermal decomposition at relatively low temperatures. These characteristics enabled it to function as a single-source precursor, offering strong support for forming $\text{Cu}_2\text{O}/\text{CeO}_2/\text{MWCNTs}$ nanocomposites.

2. Experimental

2.1. Materials

Cerium(III) nitrate hexahydrate (99.9%), 5-methyl-2-pyrazinecarboxylic acid (5mpca) (98%), and multi-walled carbon nanotube (MWCNT, 50–90 nm diameter, >95% carbon) were purchased from Sigma-Aldrich. Copper(II) acetate hydrate (98%) was purchased from Synth (Brazil). All chemicals were used as purchased, without further purification. 5-methyl-2-pyrazinehydroxamic acid (5mpzHA) was synthesized as described in the literature [3]. **MC-Ce** was synthesized following a reported method for the Eu^{III} analog [3], reacting $\text{Ce}(\text{NO}_3)_3 \cdot 6\text{H}_2\text{O}$ salt with $\text{Cu}(\text{OAc})_2 \cdot \text{H}_2\text{O}$ salt and 5mpzHA acid, as described above:

$[\text{CeCu}_5(5\text{mpzHA})_5(\text{NO}_3)(\text{H}_2\text{O})_7] \cdot 2\text{NO}_3 \cdot 7\text{H}_2\text{O}$ (**MC-Ce**): 5mpzHA (0.017 g, 0.110 mmol), and $\text{Cu}(\text{AcO})_2 \cdot \text{H}_2\text{O}$ (0.023 g, 0.110 mmol) were dissolved in methanol (10 mL) and the solution was kept under stirring at 60 °C for 1 h. A methanolic solution (10 mL) of $\text{Ce}(\text{NO}_3)_3 \cdot 6\text{H}_2\text{O}$ (0.009 g, 0.021 mmol) was added and the reaction was stirred at 60 °C for an additional 1 h. The solution color changed from brown to emerald green 15 min after adding cerium(III) salt. Thus, the solution was filtered and undisturbed at 18 °C, yielding dark green plate-like crystals within 2–4 weeks. Yield: 45%. ATR-FTIR (ν/cm^{-1}): 3355_(\nu\text{O-H}); 3239_(\nu\text{O-H}); 3033_(\nu\text{C-H}); 1604_(\nu\text{C=O}); 1580_(\nu\text{CC/CN}); 1544_(\nu\text{C-Car}); 1481_{(\nu\text{N-O(nitrate)})}; 1453_(\delta\text{C-H}); 1382_{(\nu\text{N-O(nitrate)})}; 1299, 1250_{(\nu\text{N-O(nitrate)})}; 1199_(\delta\text{C-N-O}); 1070_(\delta\text{C-H}); 1047_(\nu\text{N-O}); 991_{(\nu\text{N-O(nitrate)})}.

Copper and cerium oxides on MWCNTs were synthesized following a procedure analogous to that described in the literature [4,5] with only minor adjustments to the quantities of precursors. A quantity of MWCNTs (0.015 g) was added to aqueous metallacrown **MC-Ce** (0.015 g) in 5 mL of water, and the mixture was stirred and sonicated for 1.5 h at room temperature to obtain a suspension. The mixture was transferred to a 25 mL Teflon-lined stainless steel autoclave and heated at 190 °C for one day. The resulting precipitate was separated by centrifugation, washed with distilled water and acetone, and dried in an oven at 110 °C.

2.2. Characterization

The FT-IR spectrum was collected using a Shimadzu model FT-IR-Prestige 21 ATR and spectral scan between 4000 and 400 cm^{-1} . Thermal analyses (TGA) (Netzsch, Germany, STA 449 F3 Jupiter) were performed with the simultaneous thermal analyzer in the temperature

range 30–1100 °C by using alumina crucibles and ca. 10 mg of the sample. A dinitrogen flow of 100 cm³ min^{−1} with a heating rate of 10 °C min^{−1} was used. The Powder X-ray diffraction data were collected at room temperature using a Rigaku Ultima IV (Rigaku, Japan) with Cu-K α radiation (1.5418 Å, 40 kV, 30 mA) from 3° to 50° and 10 to 100° (2 θ) using a step size of 0.02° (Figure S1, in Supporting Information). The magnetic measurements were performed in a SQUID magnetometer (model MPMS3), Quantum Design Inc., San Diego, CA, USA) for dc magnetic measurements and a PPMS for ac magnetic susceptibility measurements, both from the Quantum Design company. Data were collected for the polycrystalline sample crushed in a VSM powder sample holder.

2.3. X-Ray Crystallography

X-ray diffraction data collection for **MC-Ce** was performed with a GEMINI-A Ultra diffractometer (Rigaku-Oxford Diffraction, USA) diffractometer equipped with Mo-K α radiation (λ = 0.71073 Å). Data integration and scaling of the reflections were performed with CrysAlisPro 1.171.40.42a [11]. Final unit cell parameters were based on the fitting of all reflection positions. Analytical absorption corrections were performed using the CrysAlisPro 1.171.40.42a. [12] Compound **MC-Ce** displayed large accessible voids, which are filled with disordered crystallization solvent molecules or counterions. Efforts to unambiguously identify all of them were unsuccessful and the solvent mask routine implemented on the Olex2 program was used [13]. One void presenting a volume of 552 Å³ was found per unit cell, accounting for 182 electrons per unit cell. This number of electrons is consistent with the presence of one nitrate and six crystallization water molecules per formula unit. This assumption is consistent with elemental analysis and thermal results. The MERCURY [14] program was used to prepare artwork representations. Crystal data and details of the data collection and refinement for **MC-Ce** are listed in Table 1. All crystallographic data are available in the supporting information section as CIF files. CCDC number is 2388656.

Table 1. Summary of the crystal data and refinement details for **MC-Ce**.

Formula	C ₃₀ H ₅₃ Cu ₅ CeN ₁₈ O ₃₃
Formula weight (g·mol ^{−1})	1651.69
Crystal system	Triclinic
Space group	P $\bar{1}$
T/K	293
Wavelength (Å)	0.71073
<i>a</i> /Å	11.6894(2)
<i>b</i> /Å	15.4536(4)
<i>c</i> /Å	16.1745(5)
α (°)	79.469(2)
β (°)	87.062(2)
γ (°)	81.301(2)
<i>V</i> (Å ³)	2838.72(13)
<i>Z</i>	2
ρ /mg cm ^{−3}	1.733
μ (mm ^{−1})	2.71
<i>F</i> (000)	1470
Crystal size (mm)	0.35 × 0.25 × 0.03
θ range/(°)	2.2–29.6
Reflns. with <i>I</i> > 2 σ (<i>I</i>)	9434
Independent reflns.	13,295
<i>R</i> _{int}	0.047
N°. of parameters/GOF on <i>F</i> ²	736/1.11
<i>R</i> , <i>wR</i> [<i>I</i> > 2 σ (<i>I</i>)]	0.045, 0.105
Largest diff. peak/hole (e Å ^{−3})	0.97/−0.79

$$w = 1/[\sigma^2(\text{Fo}^2) + (0.0405\text{P})^2 + 0.0994\text{P}] \text{ where } P = (\text{Fo}^2 + 2\text{Fc}^2)/3.$$

3. Results and Discussion

The main characteristic observed in the IR spectrum is the vibrational stretching frequency at 1604 cm^{-1} of the $\nu_{\text{C=O}}$ band, which indicates the double deprotonation of the 5mpzHA ligand and the coordination of the amide-type nitrogen and oxygen atoms to metal ions. The coordination of the ligand can also be noted by the presence of the $\nu_{\text{CC/CN}}$ at 1580 cm^{-1} as well as bands at 1480, 1398, 1337, and 1297 cm^{-1} due to the presence of nitrate anions [3].

The thermogravimetric analysis (Figure 1) shows an initial weight loss between 39 and 217°C , attributed to removing coordinated and uncoordinated water molecules, totaling 14 water molecules (obsd. 14.6; calcd. 15.3%). Subsequent weight loss steps are observed up to 900°C , likely corresponding to the decomposition of **MC-Ce**, involving the loss of nitrate anions (3 molecules) and the 5-methyl-2-pyrazinehydroximate (5mpzA^{2-} , 3 molecules), resulting in 41.4% of the compound (obsd. 38.7%). The significant residue can be associated with the presence of copper, copper oxide, and cerium oxide phases in the sample $[\text{Cu} + 2\text{Cu}_2\text{O} + \text{CeO}_2]$ [4,5], as evidenced by the PXRD analysis (Figure 2).

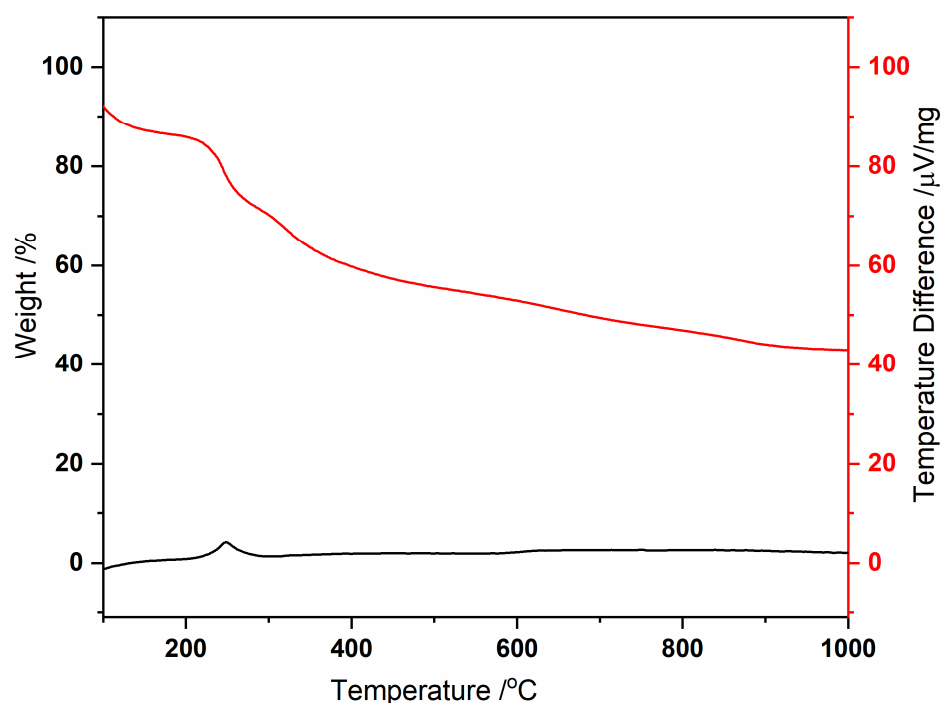


Figure 1. Thermal decomposition of **MC-Ce** under N_2 , showing TG (red) and DSC (black) curves.

In addition, our powder X-ray investigation indicates that the solid obtained from the reaction of the precursor **MC-Ce** with MWNTs contains copper and cerium oxides, as previously reported for other lanthanide-copper 15-MC-5 compounds [4,5] (see Figure 3).

Thus, our findings based on an X-ray investigation of the residue from the **MC-Ce** thermal decomposition in an inert atmosphere show the obtaining of cerium and copper oxide mixture, whose nanocomposite materials were also evidenced by reacting with the **MC-Ce** with MWCNT under hydrothermal conditions. To our knowledge, this is the third report involving metallacrown systems for preparing cerium–copper mixed oxides. Earlier, 15-MC-5 complexes and MWCNTs were used as unique precursors via a simple hydrothermal method [4,5] by S. Y. Ketkov et al. using a polynuclear metallamacrocyclic complex and $\text{Ce}(\text{H}_2\text{O})_4[15\text{MCCuGlyha-5}]\text{Cl}_3$ [4] with glycinehydroxamic acid (Glyha), as well as by I. L. Eremenko et al. [5] using a macrocycle $[\text{Ce}(\text{H}_2\text{O})_4[15\text{-MCCuRha-5}]$ with $\text{R} = \text{Glyha}$ and α -phenylalaninehydroxamic acid (Phalaha). In this case, cerium and copper oxide nanocrystals of various sizes and morphologies were obtained [5]. In our study, we employ the metallacrown $[\text{CeCu}_5(5\text{mpzHA})_5(\text{NO}_3)(\text{H}_2\text{O})_7] \cdot 2\text{NO}_3 \cdot 7\text{H}_2\text{O}$ (**MC-Ce**) lever-

aging its high solubility in mixtures of water and polar solvents, such as ethanol and methanol, as well as its decomposition properties at a relatively low temperature (around 217 °C) and under hydrothermal method also utilizing MWCNTs as templates, to achieve similar objectives.

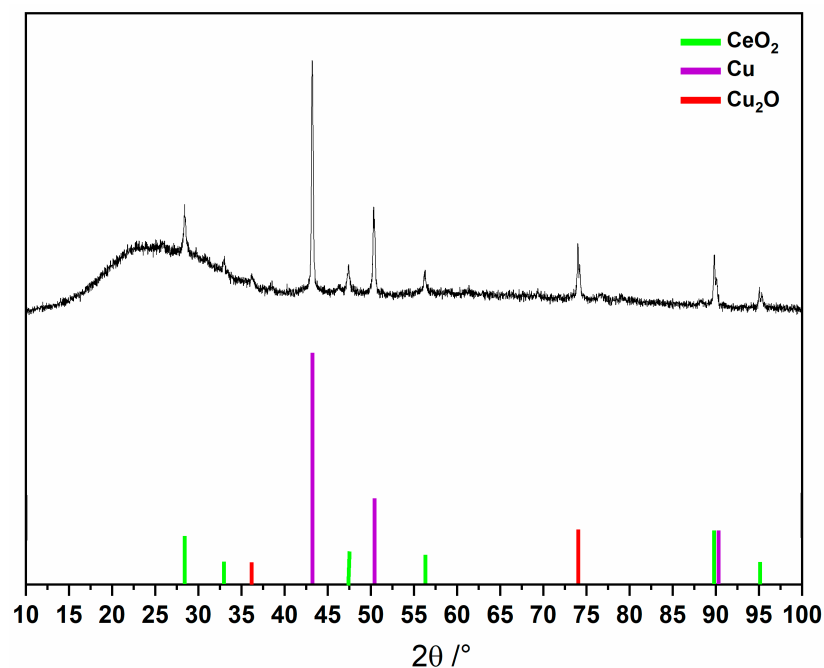


Figure 2. PXRD analysis of final product after thermal decomposition of MC-Ce.

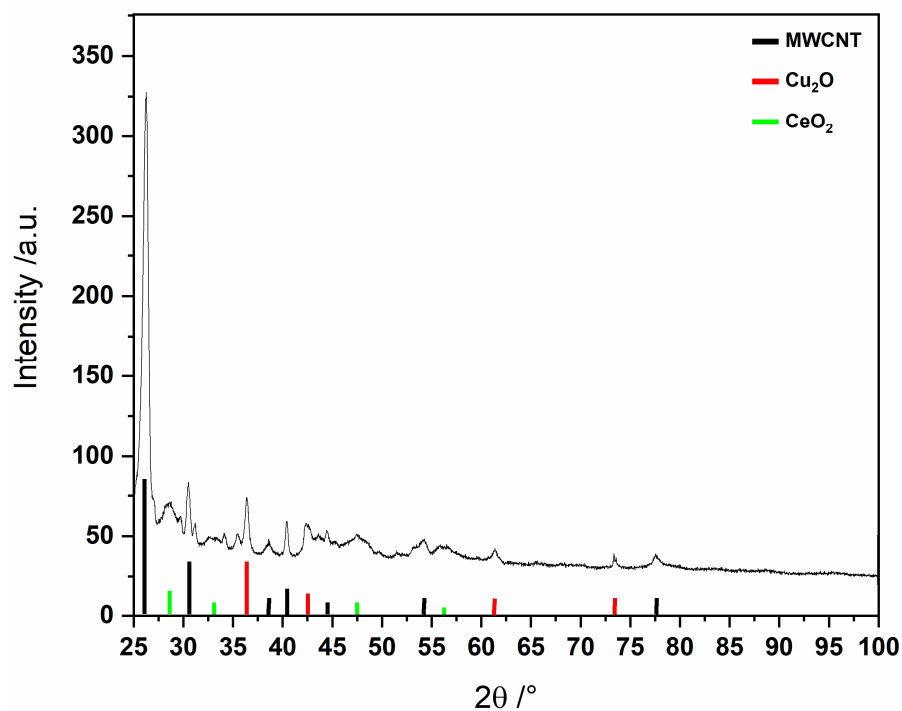


Figure 3. PXRD pattern in the presence of MWCNTs at 190 °C for 24 h using MC-Ce as a single route for nanoparticles.

In addition, PXRD experiments were also carried out with the crushed crystals of **MC-Ce**, showing a good coincidence between the experimental and calculated patterns (Figure S1, Supporting Information), confirming that the single-crystal X-ray structure is the same as the as-synthesized bulk material.

3.1. X-Ray Diffraction

The crystal structure of **MC-Ce** was solved in the centrosymmetric triclinic $P\bar{1}$ space group, probing the formation of a typical 15-MC-5 metallacrown with the general formula $[\text{CeCu}_5(5\text{mpzHA})_5(\text{NO}_3)(\text{H}_2\text{O})_7] \cdot 2\text{NO}_3 \cdot 7\text{H}_2\text{O}$. The asymmetric unit is composed of a crown-like $[\text{Cu}_5\text{Ce}(5\text{mpzHA})_5]$ core, containing five deprotonated 5mpzHA^{2-} ligands, five Cu^{II} ions, one Ce^{III} ion through a $\mu_3\text{-}\kappa^2\text{N}_2\text{N}':\kappa^2\text{O},\text{O}':\kappa\text{O}'$ chelating-bridging mode (Figure 4). Thermal ellipsoids are shown in Figure S2 (ESI).

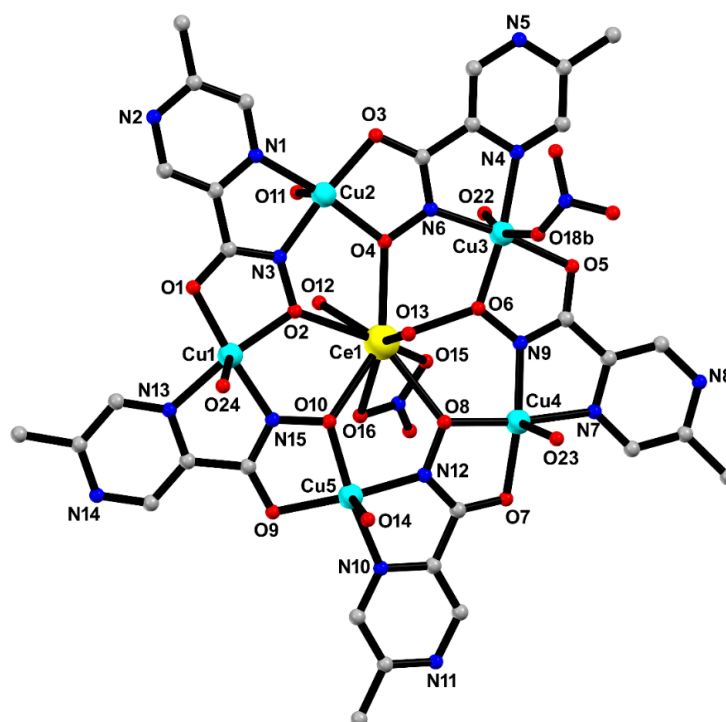


Figure 4. The asymmetric unit of **MC-Ce** with selected atom labeling. Hydrogen atoms and uncoordinated water molecules, and part of the disorder on the coordinated nitrate ion to Cu3 , were omitted for clarity. Color codes: carbon (grey), copper (cyan), oxygen (red), nitrogen (blue), and cerium (yellow).

The Ce^{III} ion is nine-coordinated to five 5mpzHA oxygen atoms, two water molecules oxygen atoms, and two nitrate group oxygen atoms, exhibiting a coordination environment of a spherical tricapped trigonal prism geometry. The SHAPE software (Version 2.1) [15] was used to determine the degree of distortion of the coordination polyhedral of the central Ce^{III} ion to **MC-Ce** concerning the ideal nine-vertex coordination polyhedral CeO_9 . The lowest continuous shape measurement (CShM) values correspond to the spherical tricapped trigonal prism (D_{3h}) (CShM = 5.874), spherical capped square antiprism (C_{4v}) (CShM = 6.649), and Muffin (C_s) (CShM = 6.549) (values in Table S1). The Ce–O bond distances in **MC-Ce** are in the range from 2.489(3) to 2.653(3) Å, where the distortion observed around the Ce^{III} geometry can be associated with the chelating nitrate ion that fills the coordination sphere, showing mostly longer bond distances [2.617(3) to 2.653(3) Å] [16].

Four copper (II) ions are pentacoordinate, exhibiting a distorted square pyramidal geometry, where each one is coordinated to the 5mpzHA ligands (basal plane) and one water molecule (apical position). The values for the trigonality parameter τ [17] are 0.11, 0.05, 0.011, and 0.042 for Cu1, Cu2, Cu4, and Cu5, respectively. The copper(II) ions are shifted from the mean basal plane by 0.043 (Cu1), 0.125 (Cu2), 0.052 (Cu3), 0.108 (Cu4), and 0.168 (Cu5) Å toward the apical position.

One copper(II) ion is coordinated to the 5mpzHA ligands in the basal plane, one water molecule, and one nitrate anion in the apical position, resulting in a distorted octahedral environment. The aqua ligands completing the copper(II) coordination sphere exhibit relatively longer bond distances [Cu1–O(24) = 2.784(4); Cu2–O(11) = 2.388(3); Cu3–O(22) = 2.531(3); Cu4–O(23) = 2.443(4); and Cu5–O(14) = 2.370(3) Å] compared to the bond distances in 5mpzHA (see Table 2).

The average shortest intramolecular Ce...Cu and Cu...Cu distances are 3.9292(6) Å and 4.5945(8) Å, respectively (Table 2). The shortest intermolecular distances between metal ions in the crystal packing are 5.8957(7) Å (Cu4...Cu5i), 6.5831(6) Å (Ce1...Cu5i), and 7.9041(5) Å (Ce1...Ce1i), where $I = 1 - x, 1 - y, 1 - z$. In addition, the O–Ce–O angles of the 5mpzHA^{2−} ligands range from 68.71(9)° (O2–Ce1–O10) to 71.68(9)° (O6–Ce–O8).

Table 2. Selected distances (in Å) for MC–Ce.

Atoms Label	Distance	Atoms Label	Distance
Cu1—N13	2.007(4)	Cu5—O9	1.944(3)
Cu1—N15	1.908(3)	Cu5—O10	1.928(4)
Cu1—O1	1.941(3)	Cu5—O14	2.370(3)
Cu1—O2	1.922(3)	Ce1—O2	2.522(3)
Cu1—O24	2.784(4)	Ce1—O4	2.489(3)
Cu2—N1	2.015(3)	Ce1—O6	2.496(3)
Cu2—N3	1.918(4)	Ce1—O8	2.502(3)
Cu2—O3	1.931(3)	Ce1—O10	2.505(3)
Cu2—O4	1.927(3)	Ce1—O12	2.530(3)
Cu2—O11	2.388(3)	Ce1—O13	2.593(3)
Cu3—N4	2.029(4)	Ce1—O15	2.617(3)
Cu3—N6	1.919(3)	Ce1—O16	2.653(3)
Cu3—O5	1.963(3)	Ce1...Cu1	3.9426(7)
Cu3—O6	1.930(3)	Ce1...Cu2	3.9567(6)
Cu3—O18b	2.69(1)	Ce1...Cu3	3.9704(8)
Cu3—O22	2.531(3)	Ce1...Cu4	3.8821(6)
Cu4—N7	1.992(3)	Ce1...Cu5	3.8944(7)
Cu4—N9	1.927(3)	Cu1...Cu2	4.5727(9)
Cu4—O7	1.946(3)	Cu2...Cu3	4.5987(8)
Cu4—O8	1.928(3)	Cu3...Cu4	4.6205(8)
Cu4—O23	2.443(3)	Cu4...Cu5	4.5929(8)
Cu5—N10	1.996(4)	Cu5...Cu1	4.5880(7)
Cu5—N12	1.919(3)		

In MC–Ce, supramolecular dimers with a Ce...Ce separation of 7.9041(5) Å are formed via a series of O–H...O hydrogen bonds [O13–H13a...O14ⁱ = 170(6)°, O13...O14ⁱ = 2.857(5) Å; O23–H23b...O24ⁱ = 172(4)°, O23...O24ⁱ = 2.855(5) Å; and O14–H14a...O23ⁱ = 156(7), O14...O23ⁱ = 2.835(5); O14–H14b...O18bⁱ = 143(5), O14...O18bⁱ = 2.711(13) (i) = 1 − x, 1 − y, 1 − z], as shown in Figure 5 (top). Moreover, a network of hydrogen bonds involving the crystallization water molecule (O25), aqua ligands (O11, O22, and O24), and the pyrazine nitrogen atoms (N5 and N14) contributed to the stabilization of the crystal packing (Figure 5, bottom). Geometric parameters for these intermolecular interactions are provided in Table S3–ESI.

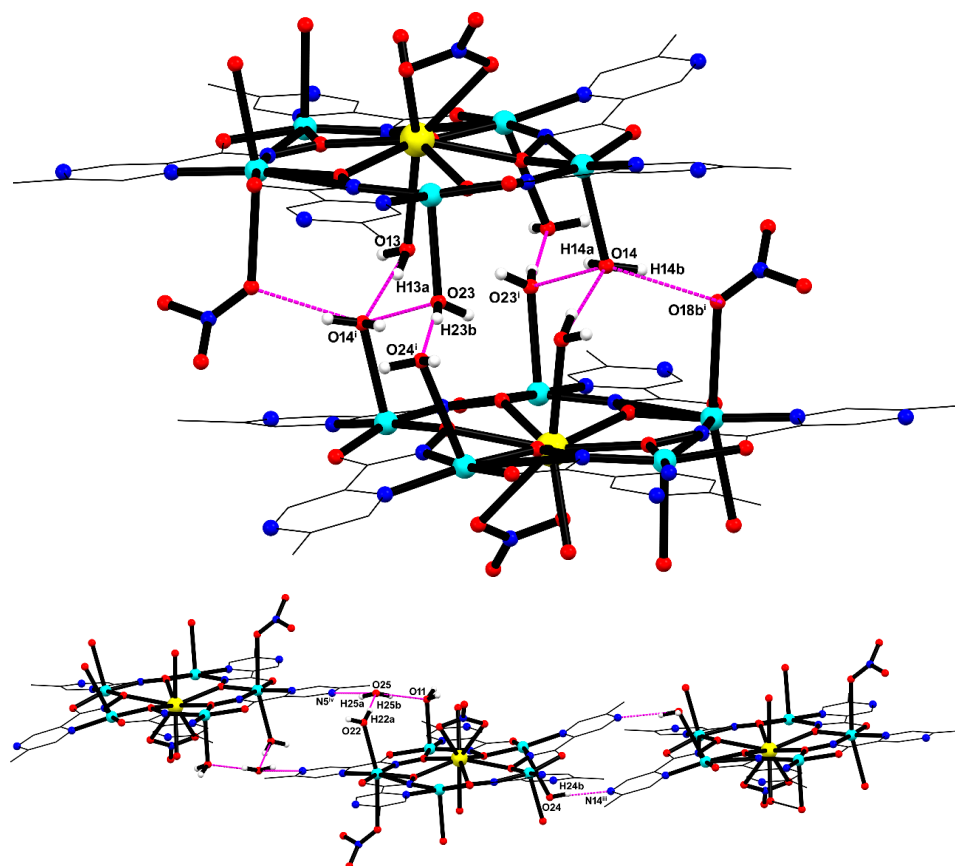


Figure 5. Supramolecular dimers are formed by hydrogen bonds involving coordinated water molecules and nitrate oxygen atom (**top**), and intermolecular interactions between crystallization water molecules, water ligands, and pyrazine nitrogen atom (**bottom**).

3.2. Magnetic Properties

dc Magnetic susceptibility was recorded in the 2–300 K temperature range for **MC-Ce** under a *dc* magnetic field of 1000 Oe. The thermal dependence of the $\chi_M T$ product is shown in Figure 6, and it has a temperature behavior similar to that observed for metallacrown with other lanthanide metallacrown complexes [3,18]. The experimental $\chi_M T$ value at room temperature is $3.175 \text{ cm}^3 \text{ mol}^{-1} \text{ K}$, which is higher than the calculated one for one magnetically isolated Ce^{III} ($J = 5/2$, $g = 6/7$, $\chi_M T = 0.80 \text{ cm}^3 \text{ mol}^{-1} \text{ K}$) plus five Cu^{II} ions ($S = 1/2$, $g = 2$, $\chi_M T = 1.875 \text{ cm}^3 \text{ mol}^{-1} \text{ K}$). Upon cooling, $\chi_M T$ decreases continuously until it reaches the value $0.80 \text{ cm}^3 \text{ mol}^{-1} \text{ K}$ at 10 K; this magnetic behavior is attributed to the antiferromagnetic interactions among Cu^{II} ions within the metallacrown hoop plus the thermal depopulation of J_Z sublevels of Ce^{III} ground state (5/2), which exhibit a small splitting under the anisotropic ligand field effects. At around 10 K, it exhibits a further slight decrease, which also suggests the presence of intramolecular antiferromagnetic interactions. The experimentally obtained $\chi_M T$ data for the **MC-Ce** were fitted using the previously reported additive model by means of the PHI program with a Hamiltonian (Equation (1)) that considers the exchange interactions between adjacent Cu^{II} ions ($\hat{H}_{\text{Ex}(\text{Cu-Cu})}$) to be dominant. The magnetic contribution of Ce^{III} was considered by adding to the fitting model a free ion approximation to account for the magnetic anisotropy by using the anisotropic Hamiltonian ($\hat{H}_{\text{CF}(\text{Ce})}$). The exchange interaction between Cu^{II} and Ce^{III} is expected to be very weak, and it was neglected to avoid overparameterization. To account for weak magnetic interactions in the system, including intermolecular magnetic

interactions and exchange interactions between Cu^{II} and Ce^{III} , a molecular field model was applied (Equation (4)):

$$\hat{H} = \hat{H}_{\text{Ex}(\text{Cu-Cu})} + \hat{H}_{\text{CF}(\text{Ce})} + \text{Zeeman terms} \quad (1)$$

$$\hat{H}_{\text{Ex}(\text{Cu-Cu})} = 2J (\hat{S}_1 \cdot \hat{S}_2 + \hat{S}_2 \cdot \hat{S}_3 + \hat{S}_3 \cdot \hat{S}_4 + \hat{S}_4 \cdot \hat{S}_5 + \hat{S}_5 \cdot \hat{S}_1) \quad (2)$$

$$\hat{H}_{\text{CF}(\text{Ce})} = B_2^0 \hat{O}_2^0 + B_4^0 \hat{O}_4^0 \quad (3)$$

$$\chi_M T = \chi_M T / [1 - (2z)' \chi_M T / N_A g^2 \mu_B^2] \quad (4)$$

in which J is the isotropic exchange interaction parameter between adjacent Cu^{II} ions in the metallacrown unit, and \hat{S}_i is the spin operator for the corresponding Cu^{II} ions. The anisotropic Hamiltonian considers the second and fourth-order axial anisotropy terms (B_2^0 and B_4^0) with the corresponding Stevens' operator equivalents (\hat{O}_2^0 and \hat{O}_4^0). As shown in Figure 6, the calculated curve (solid line) matches the experimental data in the investigated temperature range quite well. The best fit was achieved with $J = -51.8(1) \text{ cm}^{-1}$, $zJ' = -0.90(5) \text{ cm}^{-1}$, $\text{TIP} = 0.003 \text{ cm}^3 \text{ mol}^{-1}$ (TIP is the temperature-independent paramagnetism), $g_{\text{Cu}} = 2.148(2)$, and $g_{\text{Ce}} = 0.857(3)$. These values are close to previously reported data for similar metallacrown core $\text{Ln}^{\text{III}}\text{-Cu}^{\text{II}}5$ [9] obtained for the anisotropy coefficients ($B_2^0 = -13.0(2)$, $B_4^0 = -0.468(10) \text{ cm}^{-1}$), and are in the same order of values observed for other complexes based on Ce^{III} ions [18].

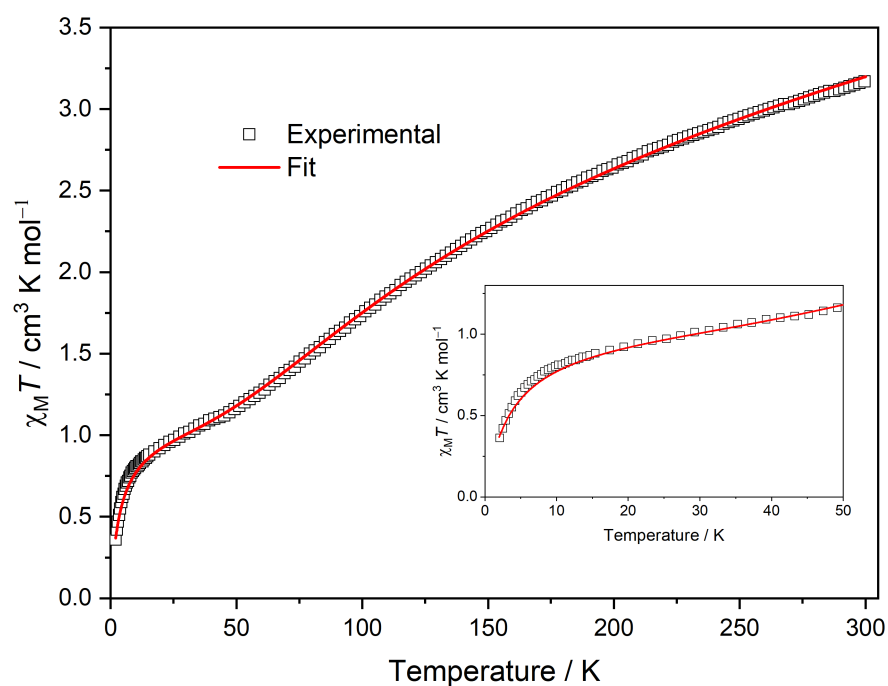


Figure 6. Temperature dependence of the $\chi_M T$ product of **MC-Ce** was measured by applying the 1 kOe dc field. The solid line is the best fit (see the main text for details). Inset: a magnified view in the temperature range of 2–50 K.

The experimental magnetic field dependence of the magnetization at three different temperatures (2, 4, and 8 K) is shown in Figure 7. When the external magnetic field reaches 7 T, the magnetization attains a maximum value of $1.45 \text{ N}\mu\text{B}$. Despite the gradual increases at a high field, no saturation of the magnetization is observed, suggesting significant anisotropy. At low temperatures, the contribution of the adjacent uncompensated Cu^{II} ion ($S = 1/2$) is expected alongside the contribution of the Ce^{III} ion ($S = 1/2$), which would result in a saturation magnetization of $2 \text{ N}\mu\text{B}$. In addition to the anisotropy effect, as highlighted in the inset of Figure 7, the large discrepancy between the experimental value

and the expected saturation magnetization value may be attributed to a frustration effect on the uncompensated Cu^{II} ions [18]. This discrepancy is evident when the simulated magnetization curves, calculated using PHI with parameters derived from the susceptibility fit, are compared to the experimental magnetization data, shown in Figure S3.

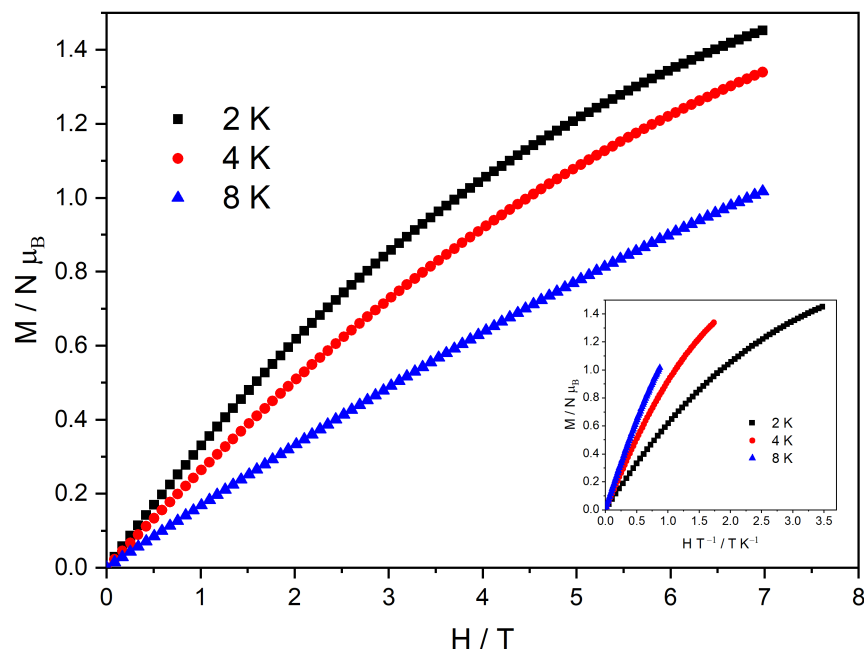


Figure 7. Isothermal M vs. H plot for complex **MC-Ce** measured at 2, 4, and 8 K. Inset: reduced magnetization plot (M vs. H/T) measured at 2, 4, and 8 K.

To explore the possible dynamics of the magnetization of the Ce–Cu5 complex, alternating current (ac) magnetic susceptibility measurements were conducted in the temperature range of 2.0–10.0 K under an applied field up to 10 kOe. This study showed the lack of any significant out-of-phase signal for **MC-Ce** under zero and non-zero applied dc fields, evidencing that the **MC-Ce** does not exhibit slow magnetic relaxation.

4. Conclusions

This work describes a new 15-MC-5 metallacrown containing Ce^{III} and Cu^{II} centers of the formula $[\text{CeCu}_5(5\text{mpzHA})_5(\text{NO}_3)(\text{H}_2\text{O})_7] \cdot 2\text{NO}_3 \cdot 7\text{H}_2\text{O}$ (**MC-Ce**). The Ce^{III} ion features a nine-vertex CeO_9 spherical tricapped trigonal prism coordination environment. The thermal analysis revealed the collapse of the structure after 217 °C, and the phase composition of the residue was determined using PXRD, showing the presence of copper and copper/cerium oxide particles. These nanocomposite materials were synthesized using the metallacrown **MC-Ce** via a hydrothermal method at 190 °C in the presence of MWCNTs, providing evidence that this metallacrown can serve as a template for the synthesis of nanoparticles. Inspired by this result, further investigations into the functionality of these nanocomposites could reveal their potential applications. The experimental $\chi_M T$ value at room temperature was $3.175 \text{ cm}^3 \text{ mol}^{-1} \text{ K}$, higher than the calculated one for one magnetically isolated Ce^{III} plus five Cu^{II} ions ($\chi_M T = 1.875 \text{ cm}^3 \text{ mol}^{-1} \text{ K}$). The $\chi_M T$ decreases continuously until it reaches the value of $0.80 \text{ cm}^3 \text{ mol}^{-1} \text{ K}$ at 10 K, where this magnetic behavior was attributed to the antiferromagnetic interactions among Cu^{II} ions within the metallacrown hoop plus the thermal depopulation of J_Z sublevels of Ce^{III} ground state (5/2), which exhibit a small splitting under the anisotropic ligand field effects.

Supplementary Materials: The following supporting information can be downloaded at: <https://www.mdpi.com/article/10.3390/magnetochemistry10120096/s1>, Figure S1. Experimental (red) and calculated (black) PXRD patterns for MC-Ce; Figure S2. Thermal ellipsoids of the asymmetric unit of MC-Ce drawn at 50% of probability. Color codes: carbon (grey), copper (cyan), oxygen (red), nitrogen (blue), and cerium (yellow); Figure S3. Isothermal magnetization (M) versus magnetic field (H) plot for MC-Ce at 2, 4, and 8~K. Table S1. Geometric analysis of the coordination environment of the cerium(III) ion in MC-Ce, showing the site symmetry approximation derived from continuous shape measures; Table S2. Selected interatomic bond angles (deg) for the MC-Ce; Table S3. Hydrogen bond observed in the supramolecular crystal packing (values in Å and deg).

Author Contributions: J.D.T. and F.F.P. contributed equally. J.D.T., F.F.P. and L.A.F. synthesized and characterized the system; R.M.R.d.S., L.D.G.B. and C.C.C. participated in the characterization by thermal analysis and Powder X-ray diffraction; I.M.L.R. and G.P.G. collected and treated single-crystal X-ray diffraction data; A.M.G. and W.C.N. collected and performed the magnetic data acquisition and processing; M.V.M. participated in supervising the synthesis, analyses, and interpretation besides writing and reviewing all the data of the paper. All authors have read and agreed to the published version of the manuscript.

Funding: This work was carried out with support from FAPEMIG and CNPq Foundations, Brazil (process number: BPQ-APQ-06579-24); FAPEMIG (CEX-APQ-01597-17, APQ-00544-23, APQ-05218-23); FAPERJ (E-26/010.000978/2019, E-26/010.1553/2019, E-26/201.314/2022); CNPq (307135/2023-3); CAPES (001); PIBIC/PIBITI_CNPq, PIBICT_Fapemig, PRPPG-UNIFAL-MG.

Data Availability Statement: The data presented in this study are available in this article or the Supplementary Materials.

Acknowledgments: The Fundação de Amparo à Pesquisa do Estado de Minas Gerais supported this work (FAPEMIG, CEX-APQ-01597-17, APQ-00544-23, APQ-05218-23). M.V.M. extends their sincere appreciation for the support provided for this project, which was carried out with support from FAPEMIG and CNPq Foundations, Brazil (process number: BPQ-APQ06579-24). C.C.C., F.F.P. and R.M.R.d.S. thank CAPES Foundation (Brazil, CAPES, finance code: 001). W.C.N. thanks FAPERJ (projects E-26/010.000978/2019 and E-26/010.1553/2019). G.P.G. thanks FAPERJ (project E-26/201.314/2022) and CNPq (project 307135/2023-3). J.D.T. and L.D.G.B. thank PIBIC/PIBITI_CNPq, PIBICT_Fapemig, and UNIFAL-MG for their undergraduate research fellowships. M.V.M. wishes to thank PROAP and PRPPG (UNIFAL-MG) and the laboratories of UNIFAL-MG: (IR spectroscopy, TG/DSC analysis (FINEP 01/10/0798/00), powder XRD Multiuser Laboratory (Labcrystal), and support of LabCRI (UFMG) for the use of SXRD diffraction facilities. M.V.M. dedicates this article to the beloved memory of great friend and Miguel Julve, whose scientific contributions and unwavering dedication to the field are incalculable. His passion for discovery and generosity in sharing knowledge continue to inspire all who had the privilege to work alongside him. He will be greatly missed both personally and professionally.

Conflicts of Interest: The authors declare no competing financial interests.

References

- Mezei, G.; Zaleski, C.M.; Pecoraro, V.L. Structural and Functional Evolution of Metallacrowns. *Chem. Rev.* **2007**, *107*, 4933–5003. [CrossRef] [PubMed]
- Lutter, J.C.; Zaleski, C.M.; Pecoraro, V.L. Metallacrowns: Supramolecular Constructs with Potential in Extended Solids, Solution-State Dynamics, Molecular Magnetism, and Imaging. In *Advances in Inorganic Chemistry*; Academic Press Inc.: Cambridge, MA, USA, 2018; Volume 71, pp. 177–246.
- Paiva, F.F.; Ferreira, L.A.; Rosa, I.M.L.; da Silva, R.M.R.; Sigoli, F.; Cambraia Alves, O.; Garcia, F.; Guedes, G.P.; Vanda Marinho, M. Heterobimetallic Metallacrown of $\text{Eu}^{\text{III}}\text{Cu}^{\text{II}}_5$ with 5-Methyl-2-Pyrazinehydroxamic Acid: Synthesis, Crystal Structure, Magnetism, and the Influence of Cu^{II} Ions on the Photoluminescent Properties. *Polyhedron* **2021**, *209*, 115–466. [CrossRef]
- Kremlev, K.V.; Samsonov, M.A.; Zabrodina, G.S.; Arapova, A.V.; Yunin, P.A.; Tatarsky, D.A.; Plyusnin, P.E.; Katkova, M.A.; Ketkov, S.Y. Copper(II)-Cerium(III) 15-Metallacrown-5 Based on Glycinehydroxamic Acid as a New Precursor for Heterobimetallic Composite Materials on Carbon Nanotubes. *Polyhedron* **2016**, *114*, 96–100. [CrossRef]
- Katkova, M.A.; Kremlev, K.V.; Zabrodina, G.S.; Rumyantsev, R.V.; Gazhulina, A.P.; Gusev, S.A.; Ketkov, S.Y.; Fomina, I.G.; Eremenko, I.L. Polynuclear Aminohydroximate Metallamacrocyclic Cu(II)-Ce(III) Complexes: A Facile Route to Intricate Nanostructures of Copper and Cerium Oxides. *Eur. J. Inorg. Chem.* **2019**, *2019*, 1002–1010. [CrossRef]
- Wada, H.; Ooka, S.; Yamamura, T.; Kajiwara, T. Light Lanthanide Complexes with Crown Ether and Its Aza Derivative Which Show Slow Magnetic Relaxation Behaviors. *Inorg. Chem.* **2017**, *56*, 147–155. [CrossRef] [PubMed]

7. Pointillart, F.; Bernot, K.; Sessoli, R.; Gatteschi, D. Effects of 3d-4f Magnetic Exchange Interactions on the Dynamics of the Magnetization of Dy^{III}-M^{II}-Dy^{III} Trinuclear Clusters. *Chem. Eur. J.* **2007**, *13*, 1602–1609. [[CrossRef](#)] [[PubMed](#)]
8. Mautner, F.A.; Bierbaumer, F.; Fischer, R.C.; Tubau, À.; Speed, S.; Ruiz, E.; Massoud, S.S.; Vicente, R.; Gómez-Coca, S. Insights into the Spin Dynamics of Mononuclear Cerium(III) Single-Molecule Magnets. *Inorg. Chem.* **2022**, *61*, 11124–11136. [[CrossRef](#)] [[PubMed](#)]
9. Pavlishchuk, A.V.; Kolotilov, S.V.; Zeller, M.; Lofland, S.E.; Addison, A.W. Magnetic Properties of Ln^{III}-Cu^{II} 15-Metallacrown-5 Dimers with Terephthalate (Ln^{III} = Pr, Nd, Sm, Eu). *Eur. J. Inorg. Chem.* **2018**, *2018*, 3504–3511. [[CrossRef](#)]
10. Le Roy, J.J.; Korobkov, I.; Kim, J.E.; Schelter, E.J.; Murugesu, M. Structural and Magnetic Conformation of a Cerocone [Ce(COT'')₂]-Exhibiting a Uniconfigurational f1 Ground State and Slow-Magnetic Relaxation. *Dalton Trans.* **2014**, *43*, 2737–2740. [[CrossRef](#)] [[PubMed](#)]
11. Rigaku Oxford Diffraction. *CrysAlisPro*; Agilent: Santa Clara, CA, USA, 2014.
12. Clark, R.C.; Clark, J.S.R. The analytical calculation of absorption in multifaceted crystal. *Acta Cryst.* **1995**, *A51*, 887–897. [[CrossRef](#)]
13. Dolomanov, O.V.; Bourhis, L.J.; Gildea, R.J.; Howard, J.A.K.; Puschmann, H. OLEX2: A Complete Structure Solution, Refinement and Analysis Program. *J. Appl. Crystallogr.* **2009**, *42*, 339–341. [[CrossRef](#)]
14. MacRae, C.F.; Sovago, I.; Cottrell, S.J.; Galek, P.T.A.; McCabe, P.; Pidcock, E.; Platings, M.; Shields, G.P.; Stevens, J.S.; Towler, M.; et al. Mercury 4.0: From Visualization to Analysis, Design and Prediction. *J. Appl. Crystallogr.* **2020**, *53*, 226–235. [[CrossRef](#)] [[PubMed](#)]
15. Llunell, M.; Casanova, D.; Cirera, J.; Alemany, P.; Alvarez, S. *SHAPE: Program for the Stereochemical Analysis of Molecular Fragments by Means of Continuous Shape Measures and Associated Tools*; Version 2.1; Universitat de Barcelona: Barcelona, Spain, 2013.
16. Costa, A.I.; da Silva, R.M.R.; Botelho, L.D.G.; Coelho, S.F.N.; Sigoli, F.A.; Honorato, J.; Ellena, J.; Martins, F.T.; Gomes, A.M.; Nunes, W.C.; et al. Intensity and Lifetime Ratiometric Luminescent Thermometer Based on a Tb(III) Coordination Polymer. *Dalton Trans.* **2024**, *53*, 3994–4004. [[CrossRef](#)] [[PubMed](#)]
17. Addison, A.W.; Rao, T.N.; Reedijk, J.; Van Rijn, J.; Verschoor, G.C. Synthesis, Structure, and Spectroscopic Properties of Copper(II) Compounds Containing Nitrogen-Sulphur Donor Ligands; the Crystal and Molecular Structure of Aqua[1,7-Bis(N-Methylbenzimidazol-2'-yl)-2,6-Dithiaheptane]Copper(II) Perchlorate. *J. Chem. Soc. Dalton Trans.* **1984**, 1349–1356. [[CrossRef](#)]
18. Hino, S.; Maeda, M.; Yamashita, K.; Kataoka, Y.; Nakano, M.; Yamamura, T.; Nojiri, H.; Kofu, M.; Yamamuro, O.; Kajiwar, T. Linear Trinuclear Zn(II)-Ce(III)-Zn(II) Complex Which Behaves as a Single-Molecule Magnet. *Dalton Trans.* **2013**, *42*, 2683–2686. [[CrossRef](#)] [[PubMed](#)]

Disclaimer/Publisher's Note: The statements, opinions and data contained in all publications are solely those of the individual author(s) and contributor(s) and not of MDPI and/or the editor(s). MDPI and/or the editor(s) disclaim responsibility for any injury to people or property resulting from any ideas, methods, instructions or products referred to in the content.